

1 Black carbon aerosol in winter northeastern Qinghai-Tibetan  
2 Plateau, China: [the source, mixing state and optical property](#)

3 **Q. Y. Wang<sup>1</sup>, R.-J. Huang<sup>1,2,3</sup>, J. J. Cao<sup>1,5</sup>, X. X. Tie<sup>1</sup>, H. Y. Ni<sup>1</sup>,**  
4 **Y. Q. Zhou<sup>1</sup>, Y. M. Han<sup>1</sup>, T. F. Hu<sup>1</sup>, C. S. Zhu<sup>1</sup>, T. Feng<sup>4,5</sup>, N.**  
5 **Li<sup>6</sup>, J. D. Li<sup>1</sup>**

6 [1] Key Laboratory of Aerosol Chemistry and Physics, Institute of Earth Environment,  
7 Chinese Academy of Sciences, Xi'an 710061, China

8 [2] Laboratory of Atmospheric Chemistry, Paul Scherrer Institute (PSI), 5232 Villigen,  
9 Switzerland

10 [3] Centre for Climate and Air Pollution Studies, Ryan Institute, National University of  
11 Ireland Galway, University Road, Galway, Ireland

12 [4] School of Human Settlements and Civil Engineering, Xi'an Jiaotong University, Xi'an  
13 710054, China

14 [5] Institute of Global Environmental Change, Xi'an Jiaotong University, Xi'an 710049,  
15 China

16 [6] National Taiwan University, Department of Atmospheric Science, Taipei 10617, Taiwan

17  
18 Correspondence to: R.-J. Huang (rujin.huang@ieecas.cn) or J. J. Cao (cao@loess.llqg.ac.cn)

19  
20 **Abstract**

21 Black carbon (BC) aerosol at high-altitude Qinghai-Tibetan Plateau has potential effects on  
22 the regional climate and hydrological cycle. An intensive measurement campaign was  
23 conducted at Qinghai Lake (~3200 [ASLmetres above sea level](#)) at the edge of the northeastern  
24 Qinghai-Tibetan Plateau during winter using a ground-based single particle soot photometer  
25 (SP2) and a photoacoustic extinctions (PAX). The average [concentration of refractory BC](#)  
26 [\(rBC\)-concentration](#) and number fraction of coated rBC were found to be  $160 \pm 190 \text{ ng m}^{-3}$   
27 and 59.3% for the entire campaign, respectively. Significant enhancements of rBC loadings

1 and number fraction of coated  $rBC$  were observed during pollution episode, with an average  
2 value of  $390 \text{ ng m}^{-3}$  and ~~64.665~~%, respectively. The mass size distribution of  $rBC$  particles  
3 showed lognormal distribution with a peak diameter of  $\sim 187 \text{ nm}$  regardless of the pollution  
4 level. Five-day backward trajectory analysis ~~combined with the fire counts map~~ suggests that  
5 the ~~biomass burning~~ air masses from North India contributed ~~ing~~ to the increased  $rBC$  loadings  
6 during the campaign. The potential source contribution function (PSCF) model combined  
7 with the fire counts map further proves that biomass burning from North India is an important  
8 potential region-source influencing northeastern Qinghai-Tibetan Plateau during the pollution  
9 episode. The  $rBC$  mass absorption cross section ( $MAC_{rBC}$ ) at  $\lambda = 532 \text{ nm}$  was slightly larger  
10 in clean days ( $14.9 \text{ m}^2 \text{ g}^{-1}$ ) than during pollution episode ( $9.3 \text{ m}^2 \text{ g}^{-1}$ ), likely due to the effects  
11 of brown carbon and the uncertainty of the  $MAC_{rBC}$  calculation. The  $MAC_{rBC}$  was positively  
12 correlated with number fraction of coated  $rBC$  during pollution episode with an increasing  
13 rate of  $0.18 (\text{m}^2 \text{ g}^{-1}) \%^{-1}$ . The number fraction of coated  $rBC$  particles showed positive  
14 correlation with light absorption, suggesting that the increase of coated  $rBC$  particles will  
15 enhance the light absorption. Compared to  $rBC$  mass concentration,  $rBC$  mixing sate is more  
16 important in determining absorption during pollution episode, estimated from the same  
17 percentagewise increment of either  $rBC$  mass concentration or the number fraction of coated  
18  $rBC$ . The estimated BC direct radiative forcing was  $+0.93 \text{ W m}^{-2}$  for pollution episode, which  
19 is 2 times larger than that in clean days. Our study provides insight into the potential climatic  
20 impacts of  $rBC$  aerosol transported to the Qinghai-Tibetan Plateau from South Asian regions,  
21 and is also useful for future modeling studies.

## 23 1 Introduction

24 Black carbon (BC) aerosol has received worldwide concern due to its effects on climate and  
25 human health (Anenberg et al., 2012; Bond et al., 2013). BC shows an overall warming effect  
26 by either absorbing incoming solar radiation in the atmosphere or by reducing the albedo of  
27 surface (i.e., snow and ice) (Jacobson, 2001; Ramanathan and Carmichael, 2008; Kühn et al.,  
28 2014). A total climate forcing of BC particles is estimated to be  $+1.1 \text{ W m}^{-2}$ , which is ranked  
29 as the second largest contributor to anthropogenic radiative forcing after carbon dioxide in the  
30 present-day atmosphere (Bond et al., 2013). BC particles, derived from incomplete  
31 combustion of fossil fuels or biomass, are mainly hydrophobic when emitted, but become  
32 hygroscopic over time due to atmospheric aging processes. When BC particles are mixed with

1 water-soluble aerosol composition, they can serve as cloud condensation nuclei and therefore  
2 affect microphysical properties of clouds leading to indirect effect on climate (Hansen et al.,  
3 [2005; Lohmann and Feichter, 2005](#)). [BC also shows semi-direct effect through interaction](#)  
4 [with cloud processes \(Koch and Del Genio, 2010\)](#). Moreover, the impacts of BC aerosols on  
5 the radiative balance may lead to far-reaching consequences, such as global dimming (Wild et  
6 al., 2007), lower crop yields (Tollefsen et al., 2009), and negative impacts on terrestrial and  
7 aquatic ecosystems (Forbes et al., 2006).

8 The Qinghai-Tibetan Plateau is known as the “Third Pole” of the Earth because of its  
9 immense area and high elevation. It covers the area of 27–45 °N, 70–105 °E with an average  
10 elevation >4000 m ASL (above sea level). Due to the special landform, ecosystem and  
11 monsoon circulation, the Qinghai-Tibetan Plateau exerts profound effects on regional and  
12 global radiative budget and climate (Kopacz et al., 2011; Su et al., 2013; Yang et al., 2014).  
13 The Qinghai-Tibetan Plateau is surrounded by many important anthropogenic BC aerosol  
14 source areas (Zhang et al., 2009), such as South Asia (e.g., India) and East Asia (e.g., China).  
15 Inventory study suggests that the BC emissions in China and India have increased by 40%  
16 and 54% from 2000 to 2008, respectively (Kurokawa et al., 2013). Due to the general  
17 circulation patterns, the Qinghai-Tibetan Plateau becomes a strong receptor of these high BC  
18 source areas (Cao et al., 2010; Xia et al., 2011; Cong et al., 2013; Zhao et al., 2013). Lu et al.  
19 (2012) shows that South Asia and East Asia are the main source regions, accounting for 67%  
20 and 17% of BC transported to the Himalayas and Qinghai-Tibetan Plateau on an annual basis,  
21 followed by former USSR (~8%), Middle East (~4%), Europe (~2%), and Northern Africa  
22 (~1%). Deposition of BC on snow and ice at the Qinghai-Tibetan Plateau would decrease the  
23 snow surface albedo (Xu et al., 2012; Ming et al., 2013). The Qinghai-Tibetan Plateau  
24 Glaciers, which are the largest glaciers outside of the Polar Regions, have shown signs of  
25 retreat (Xu et al., 2009). The snowmelt from Qinghai-Tibetan Plateau vitally affects the  
26 sustaining seasonal water availability leading to agriculture security in South, East, and  
27 Southeast Asia (Immerzeel et al., 2010).

28 The effect of BC transported from surroundings on Qinghai-Tibetan’s environment and  
29 climate is of great significance. However, BC studies are still very scarce to date in the  
30 Qinghai-Tibetan Plateau (e.g., Cao et al., 2010; Zhao et al., 2013; Wang et al., 2014a). In  
31 these limited studies, online and offline filter-based techniques are often used. Due to inherent  
32 systematic limitations, direct examination of BC size distribution and mixing state with filter-

1 based measurements is not feasible (Watson et al., 2005; Slowik et al., 2007; Collaud Coen et  
2 al., 2010; Bond et al., 2013). The BC optical properties are dependent on its physical (e.g.,  
3 size and shape) and chemical (e.g., mixing with other materials) features. For example, the  
4 degree of enhancement in mass absorption cross section from internal mixture of BC with  
5 other aerosol components can lead to large difference in the prediction of global radiative  
6 budget (Bond et al., 2006; Chung et al., 2012; Zhuang et al., 2013). Consequently, accurate  
7 characterization of BC particles is crucial for a precise estimate of the impacts of BC on the  
8 atmospheric radiative forcing, human health, and air quality. In this study, a single particle  
9 soot photometer (SP2) and a photoacoustic extinctions (PAX) were used to investigate the  
10 refractory black carbon (rBC) mass concentrations, size distribution, mixing state, and aerosol  
11 light absorption properties in northeastern Qinghai-Tibetan Plateau. The primary objectives of  
12 this study were (1) to investigate the important potential rBC source regions responsible for  
13 the high wintertime rBC concentration in the Northeastern Qinghai-Tibetan Plateau, (2) to  
14 study the effect of rBC mixing state on light absorption properties, (3) to estimate the direct  
15 radiative forcing during rBC pollution episode.

## 16 **2 Methodology**

### 17 **2.1 Measurement site**

18 Qinghai Lake (36.53–37.25 °N and 99.6–100.78 °E), the largest saline lake in China, is  
19 located ~3200 m ASL in a drainage closed intermountain basin on the Northeast Qinghai-  
20 Tibetan Plateau with an area of ~4400 km<sup>2</sup> (Figure 1). This region is highly sensitive to global  
21 climate change, because it is situated in the sensitive semi-arid zone between the Asian  
22 monsoon-controlled area and the westerly jet stream-influenced area (An et al., 2012).  
23 Intensive measurements were taken from 16–27 November, 2012 from the rooftop (~15 m  
24 above ground level) of a sampling tower at the “Bird Island” peninsula (36.98 °N, 99.88 °E),  
25 which is located at the northwest section of the Qinghai Lake shore as shown in Figure 1.

### 26 **2.2 rBC mass and mixing state measurements**

27 The commercially available SP2 instrument (Droplet Measurement Technology, Boulder, CO,  
28 USA) has proven useful for measuring rBC mass, size, and mixing state (e.g., Gao et al., 2007;  
29 Moteki and Kondo, 2007; Schwarz et al., 2010; Wang et al., 2015). The operating principles  
30 of the SP2 are described elsewhere (Stephens et al., 2003; Schwarz et al., 2006). Briefly, the

1 SP2 relies on laser-induced incandescence to quantify the  $r_{BC}$  mass of individual particles.  
2 Continuous intracavity Nd:YAG laser light at 1064 nm is used to heat  $r_{BC}$ -containing  
3 particles to their vaporization point. The peak incandescence signal is linearly related to the  
4  $r_{BC}$  mass in the particle irrespective of the particle morphology or mixing state; this holds  
5 true over most of the  $r_{BC}$  mass range typically observed in the accumulation mode (Slowik et  
6 al., 2007). In this work, the  $r_{BC}$  mass in the range of ~0.4–1000 fg, equivalent to ~70–1000  
7 nm volume equivalent diameter (VED), is quantified, assuming a void-free density of 2.0 g  
8  $\text{cm}^{-3}$  (Schwarz et al., 2008). This range covers >90% of the  $r_{BC}$  mass in the accumulation  
9 mode. The incandescence signal was calibrated using a standard fullerene soot sample (Lot  
10 F12S011, Alpha Aesar, Inc., Ward Hill, Massachusetts). The total uncertainty in the  $r_{BC}$   
11 mass determination was ~25%. More details about the SP2 calibration and uncertainty can be  
12 found in our previous work (Wang et al., 2014a). Note that the SP2 only quantifies the most  
13 refractory and most efficient light-absorbing component of combustion aerosol. The  $r_{BC}$   
14 concentration is adjusted to standard temperature and pressure (STP,  $T_{\text{standard}} = 273.15$  K and  
15  $P_{\text{standard}} = 1013.25$  hPa).

16 The SP2 is capable of determining the  $r_{BC}$  mixing state. The time delay between the peaks  
17 from the scattered light and incandescence signals is an indicator of the amount of non- $r_{BC}$   
18 material mixed internally with individual  $r_{BC}$  particles (Schwarz et al., 2006; McMeeking et  
19 al., 2011; Perring et al., 2011; Wang et al., 2014a). This method is sensitive to optically  
20 significant amounts of non- $r_{BC}$  material. The time delay occurs because the coatings must be  
21 removed from the  $r_{BC}$  particle before the onset of incandescence. Because the scattering  
22 measurement is rather noisy for small particles and become saturation for large particles, the  
23 mixing state was studied for  $r_{BC}$  core between ~70 and ~275 nm VED, which constitute the  
24 majority of  $r_{BC}$  particle numbers (Wang et al., 2014a). The limitation of SP2 instrument is  
25 discussed in Taylor et al. (2015) when considering leading-edge scattering. The number  
26 fraction of coated  $r_{BC}$  particles which is calculated from the distribution of time delay is an  
27 indicator of the degree to which the  $r_{BC}$  particles are coated with other substances. This  
28 number fraction is higher for more aged  $r_{BC}$  particles due to the formation of coating from  
29 atmospheric physical and chemical processes including coagulation, condensation, and  
30 heterogeneous reactions (Liu et al., 2013; Browne et al., 2015).

## 2.3 Particle light absorption measurements

The PAX (Droplet Measurement Technology, Boulder, CO, USA) measures light absorption and scattering coefficients simultaneously using a modulated diode laser. The light absorption coefficient is measured based on the intracavity photoacoustic technology. A laser beam in the acoustic chamber of the instrument heats suspended absorbing particles, by which a pressure wave is produced and detected with a sensitive microphone. A wide-angle integrating reciprocal nephelometer in the acoustic chamber measures the light scattering coefficient regardless of the particles' chemical makeup, mixing state, or morphology. In this study, the light absorption at  $\lambda = 532$  nm is measured. Before sampling, nitrogen dioxide ( $\text{NO}_2$ ) and ammonium sulfate are used for the calibration of light absorption and scattering, respectively. The PAX can provide the light extinction coefficient independently using the laser power.  $\text{NO}_2$  was used to produce an absorption reading of  $\sim 500\text{--}30000$   $\text{Mm}^{-1}$ . A correction factor was then established from the relationship between the calculated light extinction coefficient using laser power and the measured light absorption. The uncertainty of the PAX is estimated to be  $\sim 10\%$ . Like SP2 measurement, the absorption measurement reported here is also corrected for the standard temperature and pressure.

## 3 Results and discussion

### 3.1 Mass, size and mixing state of rBC aerosol

The time series of hourly averaged rBC mass concentrations and the mixing state obtained during the campaign are shown in Figure 2, and a statistical summary of the data is presented in Table 1. The mean concentration of rBC aerosol ( $\pm$  standard deviation) was  $160 \pm 190$   $\text{ng m}^{-3}$  during the entire campaign period, ranging from  $6$   $\text{ng m}^{-3}$  to  $1040$   $\text{ng m}^{-3}$ . The mean number fraction of coated rBC is found to be  $59.3 \pm 76.9\%$  (range  $39.840\text{--}73.2\%$ ), suggesting the majority of aged rBC particles in wintertime in the Qinghai Lake region. It is found that  $\sim 3025\%$  of the rBC values are higher than the mean-75th value, and the variation coefficient (defined by  $\text{SD}/\text{mean}$ ) of rBC values reaches as high as 120%, suggesting a large rBC burden even at the free tropospheric altitude. ~~It is found that  $\sim 30\%$  of the BC values are higher than the mean value, and the variation coefficient (defined by  $\text{SD}/\text{mean}$ ) of BC values reaches as high as 120%, suggesting a large BC burden even at the free tropospheric altitude.~~ Elevated rBC concentration was observed from 19 to 21 November (defined as a pollution episode hereafter) with an average rBC loading of  $390$   $\text{ng m}^{-3}$ , which is about 4 times higher than that

1 from the rest of measurement period ( $86 \text{ ng m}^{-3}$ , defined as clean days). The mean number  
2 fraction of coated  $rBC$  also increases to 64.665% during the pollution episode, higher than  
3 that in the clean days (57.758%). Given that local  $rBC$  emissions in the Qinghai Lake region  
4 and even the entire Qinghai-Tibetan Plateau are very limited, the enhanced  $rBC$   
5 concentrations observed during this campaign are most likely from regional transport as  
6 discussed below.

7 Figure 3 shows the mass size distribution of  $rBC$  particles for the entire campaign period. A  
8 lognormal size distribution pattern in VED for the size of  $rBC$  core of a particle is found, with  
9 a very close peak diameter for  $rBC$  pollution episode (188 nm) and clean days (187 nm). The  
10 size distributions of  $rBC$  core in the ambient atmosphere are affected by the size of fresh  $rBC$   
11 particles and the subsequent atmospheric processing (Bond et al., 2013). The growth of  $rBC$   
12 particles is a complex process, including water accretion, coagulation, condensation, and the  
13 accumulation of other materials through heterogeneous reactions. However, only the process  
14 of coagulation can lead to the increase of  $rBC$  core in VED. The coagulation of particles in  
15 ambient air is dominated by Brownian motion, a slow process for particles in the  
16 accumulation mode (Seinfeld and Pandis, 1998). Therefore, the similarity in VED size  
17 distribution for  $rBC$  core between clean and pollution episode indicates that the measured  $rBC$   
18 particles are likely from biomass burning emissions, given that fossil fuel and biomass  
19 burning tend to have different  $rBC$  size distributions and that the peak diameter measured in  
20 this study is similar to the reported  $rBC$  peak diameter from biomass burning plumes (range  
21  $\sim 187\text{--}193 \text{ nm}$ , see Kondo et al., 2011; Sahu et al., 2012; Taylor et al., 2014).

### 22 3.2 $rBC$ potential pollution source areas

23 To examine the contribution of regional  $rBC$  transport, five-day back trajectories were  
24 calculated using the hybrid single-particle Lagrangian integrated trajectories (HYSPLIT)  
25 model (<http://ready.arl.noaa.gov/HYSPLIT.php>~~www.arl.noaa.gov/reday.html~~). The HYSPLIT  
26 model was driven with full vertical dynamics using gridded meteorological data (Global Data  
27 Assimilation System, GDAS1). ~~was used to compute the five-day back trajectories using BC~~  
28 ~~as a marker. The five-day period is chosen because the atmospheric lifetime of BC is typically~~  
29 ~~in the order of one week (Chung and Seinfeld, 2005; Cape et al., 2012).~~ Figure 4a shows the  
30 hourly results of backward trajectories calculated with the arrival height of 100, 500 and 1000  
31 m above ground level. The  $rBC$  data were averaged to 1 hr in order to match the timestep of  
32 the trajectories. The different arrival height of trajectories shows similar transport directions,



1 suggesting the air masses mixed well at different altitude. During  $rBC$  pollution episode, the  
2 air masses were mainly originated from the regions of high  $rBC$  emissions in North India  
3 (Sahu et al., 2008), which then passed over the rather clean western Qinghai-Tibetan Plateau  
4 (Zhang et al., 2009). In contrast, the air masses were originated from Europe and passed  
5 through the western part of China during clean days. ~~An aerosol optical depth (AOD) map,~~  
6 ~~retrieved from the measurements of Moderate Resolution Imaging Spectroradiometer~~  
7 ~~(MODIS) on the Terra satellite, describes the mean atmospheric aerosol loading around~~  
8 ~~Qinghai-Tibetan Plateau (Figure 5a). Since 5-day back trajectory analysis shows that the~~  
9 ~~polluting air masses arriving the measurement site on 19–21 November were from North~~  
10 ~~India, the pollution status of North India on 14–16 November (i.e., 5 days backward) was~~  
11 ~~examined. As shown in Figure 5a, high AOD values can be found along the Indo-Gangetic~~  
12 ~~Basin in India and South Pakistan, indicating heavy pollution in this region. The fire counts~~  
13 ~~map obtained from MODIS observation on NASA satellites also shows a large number of~~  
14 ~~biomass burning activities in North India during 14–16 November, indicating large biomass~~  
15 ~~burning aerosol (including BC aerosol) emissions. Although the high altitude of the~~  
16 ~~Himalayas was thought to be a physical wall for atmospheric pollutants, previous studies~~  
17 ~~indicate that the high Himalayan valleys can act as a “direct channel” for the transport of air~~  
18 ~~pollutants up to 5000 m ASL (e.g., Bonasoni et al., 2010). After reaching the north of the~~  
19 ~~Himalayan, the air pollutants can further transport to the central Qinghai-Tibetan Plateau~~  
20 ~~(Hindman and Upadhyay, 2002; Xia et al., 2011). Therefore, the BC pollution episode~~  
21 ~~observed in the Qinghai Lake measurement site is most likely derived from the biomass~~  
22 ~~burning emissions in North India.~~

23 The potential source contribution function (PSCF) model (e.g., Wang et al., 2006) was used  
24 to further explore the potential source regions which influence  $rBC$  concentration in the  
25 Qinghai Lake region. To do so, the geographic region covered by the trajectories was divided  
26 into an array of  $0.5 \times 0.5$  degree grid cells. The PSCF values for the grid cells were calculated  
27 by counting the trajectory segment endpoints that terminate within each cell. The number of  
28 endpoints that fall in the  $ij$ th cell is designated as  $n_{ij}$ . The number of endpoints for the same  
29 cell corresponding to  $rBC$  concentrations higher than an arbitrarily set criterion is defined to  
30 be  $m_{ij}$ . Then, the PSCF value for the  $ij$ th cell is defined as:  $PSCF_{ij} = m_{ij}/n_{ij}$ . Because of the  
31 impact of small values of  $n_{ij}$ , an arbitrary weight function  $W_{ij}$  was used to better reflect the  
32 uncertainty in the values for these cells (Polissar et al., 1999). The weight function reduces the  
33 PSCF values when the total number of the endpoints in a particular cell is less than about



1 three times the average value of the end points per each cell. Here,  $W_{ij}$  is defined as (Polissar  
2 et al., 2001):

$$3 \quad W_{ij} = \begin{cases} 1.00 & 80 < n_{ij} \\ 0.70 & 20 < n_{ij} \leq 80 \\ 0.42 & 10 < n_{ij} \leq 20 \\ 0.05 & n_{ij} \leq 10 \end{cases} \quad (1)$$

4 Although PSCF model is often used to determine the potential source regions (e.g., Wang  
5 et al., 2006; Heo et al., 2013; Zhang et al., 2013), a limitation of this model is that grid cells  
6 can have the same PSCF value when sample concentrations at the receptor site are either only  
7 slightly higher or extremely higher than the criterion. This may lead to difficulties in  
8 distinguishing moderate sources from strong ones. To compensate for this limitation, the  
9 PSCF result calculated from the 75th percentile of all the data is set as the criterion ( $170 \text{ ng m}^{-3}$ )  
10 <sup>3</sup>) in this study. Figure 4b shows the map of PSCF results for the entire campaign period. High  
11 PSCF values are found at North India. The PSCF values are low in the Qinghai Lake and  
12 surrounding regions, indicating lower likelihood of high rBC emissions from local sources  
13 compared to regional transport from North India. An aerosol optical depth (AOD) map,  
14 retrieved from the measurements of Moderate Resolution Imaging Spectroradiometer  
15 (MODIS) on the Terra satellite, describes the mean atmospheric aerosol loading around  
16 Qinghai-Tibetan Plateau (Figure 5a). High AOD values can be found along the Indo-Gangetic  
17 Basin in India and South Pakistan, indicating heavy pollution in this region. The fire counts  
18 map (Figure 5b) obtained from MODIS observation on NASA satellites also shows a large  
19 number of biomass burning activities in North India, indicating large biomass burning aerosol  
20 (including rBC aerosol) emissions. Although the high altitude of the Himalayas was thought  
21 to be a physical wall for atmospheric pollutants, previous studies indicate that the high  
22 Himalayan valleys can act as a “direct channel” for the transport of air pollutants up to 5000  
23 m ASL (e.g., Bonasoni et al., 2010). After reaching the north of the Himalayan, the air  
24 pollutants can further transport to the central Qinghai-Tibetan Plateau (Hindman and  
25 Upadhyay, 2002; Xia et al., 2011). Therefore, the rBC pollution episode observed in the  
26 Qinghai Lake measurement site is most likely derived from the biomass burning emissions in  
27 North India.

### 3.3 Optical properties of rBC aerosol

The hourly light absorption coefficient varied from 0.0 to  $18.1 \text{ Mm}^{-1}$  with an average value of  $2.1 \pm 2.4 \text{ Mm}^{-1}$  for the entire campaign (Figure 2). The average value increased to  $3.7 \pm 2.9 \text{ Mm}^{-1}$  during rBC pollution episode, which is ~3 times higher than the average value in clean days ( $1.3 \pm 1.6 \text{ Mm}^{-1}$ ). The rBC mass absorption cross section ( $\text{MAC}_{\text{rBC}}$ , expressed here in  $\text{m}^2 \text{ g}^{-1}$ ) is one of the most important optical properties for rBC aerosol because this parameter links optical properties to rBC mass. The  $\text{MAC}_{\text{rBC}}$  can be calculated by dividing the absorption coefficient measured with the PAX by the rBC mass concentration from the SP2 ( $\text{MAC}_{\text{rBC}} = [\text{Absorption}]/[\text{rBC}]$ ). Due to the difference in cutoff size for PAX ( $< 2.5 \mu\text{m}$ ) and for SP2 ( $< 1.0 \mu\text{m}$ ), the  $\text{MAC}_{\text{rBC}}$  may be overestimated by ~13% given that BC concentration in  $\text{PM}_{1.0}$  accounted for ~85% of  $\text{PM}_{2.5}$  in the Tibetan Plateau (Wan et al., 2015).

Figure 6a and b show histograms of the  $\text{MAC}_{\text{rBC}}$  values during clean days and pollution episode, respectively. The distribution of  $\text{MAC}_{\text{rBC}}$  in clean days tends to larger values than that during pollution episode, with an average value of  $14.9 \pm 8.9 \text{ m}^2 \text{ g}^{-1}$  for clean days and  $9.3 \pm 3.1 \text{ m}^2 \text{ g}^{-1}$  for pollution episode. These values are higher than the  $\text{MAC}_{\text{rBC}}$  of  $7.8 \text{ m}^2 \text{ g}^{-1}$  for uncoated rBC particles (interpolated to 532 nm from 550 nm assuming an Absorption Ångström Exponent of 1.0) suggested by Bond and Bergstrom (2006). It is interesting that the  $\text{MAC}_{\text{rBC}}$  in clean days is ~60% larger than that during pollution episode, the reason for which is not clear. A possible explanation involves the interference from brown carbon. Previous studies demonstrate that brown carbon, like black carbon, is an important light-absorbing aerosol composition in the atmosphere which can absorb light at visible wavelength (e.g.,  $\lambda = 532 \text{ nm}$ ) (Yang et al., 2009). In the rural areas of Qinghai, biofuels including yak and sheep dung, firewood, and crop residues account for ~80% of total household energy (Ping et al., 2011). Biofuel/biomass combustion emissions are considered as especially significant sources for brown carbon (Andreae and Gelencser, 2006). It may produce enough brown carbon (particularly during the smoldering combustion phase) influencing the light absorption when rBC loading is low. Thus, the  $\text{MAC}_{\text{rBC}}$  may be overestimated in clean days. In addition, the calculation method using the light absorption and rBC mass may also introduce uncertainty, especially when rBC concentration is low. The high  $\text{MAC}_{\text{rBC}}$  values always correspond to the very low rBC mass. The  $\text{MAC}_{\text{rBC}}$  calculation method can bring ~30% uncertainty estimated from the square root of uncertainties in the PAX (10%) and SP2 (25%) measurements.

1 To further investigate the effect of rBC mixing state on  $MAC_{rBC}$ , the  $MAC_{rBC}$  values were  
2 plotted against the number fraction of coated rBC. As shown in Figure 7, the  $MAC_{rBC}$  was not  
3 correlated with the number fraction of coated rBC during clean days, but positive correlation  
4 was observed during pollution episode suggesting that the mixing state leads to the increase of  
5 the  $MAC_{rBC}$ . The slope of  $0.18 \text{ (m}^2 \text{ g}^{-1}) \%^{-1}$  obtained from the linear regression is arguably  
6 representative of the rate of the mixing state effect on the  $MAC_{rBC}$ .

7 Both laboratory studies and field measurements have shown that the BC light absorption  
8 (related to its direct radiative effects) can be enhanced by a factor of 1.5–2.0 when BC  
9 particles are internally mixed with other non-light-absorbing aerosol components including  
10 sulfate, nitrate, organics and water (e.g., Bond et al., 2006; Shiraiwa et al., 2010; Wang et al.,  
11 2014b). This is because the non-absorbing materials act like a lens and therefore refract the  
12 light toward the absorbing BC core, leading to the enhancement of absorption on visible light.  
13 Figure 8 shows the relationship between light absorption and rBC mixing state during clean  
14 days and pollution episode. In clean days the light absorption shows no significant correlation  
15 with number fraction of coated rBC, which could be attributed to the influences of brown  
16 carbon. In contrast, during pollution episodes the light absorption coefficients generally  
17 increase with increasing number fraction of coated rBC with the latter being positively  
18 correlated with the rBC mass concentration during pollution episode (see Figure 8b). Such  
19 correlation indicates that the outflow from polluted south Asia would increase the rBC mass  
20 concentration leading to light absorption enhancement on the one hand, and the increased  
21 number fraction of coated rBC particles would further enhance the light absorption on the  
22 other hand. To further investigate whether rBC concentration or mixing state is more  
23 important for determining absorption, the increases in light absorption are compared based on  
24 the same percentagewise increment of either rBC mass concentration or number fraction of  
25 coated rBC. According to the regression function in Figure 8b and the correlation between  
26 absorption and rBC mass (Absorption =  $-0.38 + 10.17[rBC]$ ,  $r = 0.92$ ), the increase of light  
27 absorption is larger for number fraction of coated rBC (e.g.  $\Delta$  light absorption =  $1.8 \text{ Mm}^{-1}$ )  
28 than for the rBC mass (e.g.  $\Delta$  light absorption =  $0.5 \text{ Mm}^{-1}$ ), suggesting that, compared to rBC  
29 mass concentration, rBC mixing state is more important in determining absorption during  
30 pollution episode.

### 1 3.4 Implications for direct radiative forcing

2 The direct radiative forcing of BC particles ( $DRF_{BC}$ ) refers to the change in energy balance at  
3 the top of the atmosphere due to absorption and scattering of sunlight by BC particles. Here  
4 the  $DRF_{BC}$  is estimated from a simple analytical solution derived from the following  
5 parameterization (Chylek and Wong, 1995):

$$6 \quad DRF_{BC} = \frac{S_0}{4} T_{atm}^2 \times (1 - N) \times [4\alpha\delta_{ab} - 2 \times (1 - \alpha)^2 \beta\delta_{sc}] \quad (2)$$

7 where  $S_0$  is the solar irradiance ( $1370 \text{ W m}^{-2}$ ),  $T_{atm}$  is the atmospheric transmission (0.79),  $N$  is  
8 the cloud fraction (0.6),  $\alpha$  is the surface albedo (i.e., 0.18 at rural region),  $\beta$  is the backscatter  
9 fraction, which is assumed to be 0.17 (Kim et al., 2012), and  $\delta_{ab}$  and  $\delta_{sc}$  are the absorption and  
10 scattering optical depth, respectively. The daily values of  $\delta_{ab}$  and  $\delta_{sc}$  are estimated from Aura-  
11 OMI satellite measurements (<http://disc.sci.gsfc.nasa.gov/>). More details about the  
12 assumption of this equation can be found in Kim et al. (2012). The average  $DRF_{BC}$  is  
13 estimated to be  $0.6 \pm 0.4 \text{ W m}^{-2}$  for the entire campaign, ranging from 0.05 to  $1.6 \text{ W m}^{-2}$ .  
14 During rBC pollution episode, the  $DRF_{BC}$  was  $0.93 \pm 0.57 \text{ W m}^{-2}$ , which is about two times  
15 higher than that in clean days ( $0.48 \pm 0.29 \text{ W m}^{-2}$ ). It should be noted that the  $DRF_{BC}$  is  
16 calculated based on the assumption that BC particles are externally mixed with other non-  
17 light-absorbing particles. Given that a fraction of BC particles may be internally mixed with  
18 other aerosol compounds, the  $DRF_{BC}$  calculated here should be considered as the lower limit.  
19 Therefore, the BC mediated radiative forcing is of great importance for the local atmospheric  
20 radiative balance in the northeastern Qinghai-Tibetan Plateau. Given the much shorter  
21 lifetime of BC aerosol compared with greenhouse gases, mitigation of BC pollution could be  
22 an efficient control strategy for protecting the vulnerable environment in the Qinghai-Tibetan  
23 Plateau because it reduces the radiative forcing directly by reducing the BC particle  
24 concentration and indirectly by slowing down the melting of snowpack and ice that can reflect  
25 the sunlight. It is worth to note that the rBC concentration during pollution episode was 4  
26 times higher than that in clean days, but the  $DRF_{BC}$  was only enhanced by a factor of two,  
27 suggesting the importance of other aerosol components which made negative contribution to  
28 DRF.

## 1 4 Conclusions

2 The mass concentration, size distribution, mixing state and optical properties of rBC particles  
3 in the Qinghai Lake region of the Qinghai-Tibetan Plateau are studied. The results show that  
4 average rBC concentration and number fraction of coated rBC are  $160 \pm 190 \text{ ng m}^{-3}$  and  
5 ~~59.3%~~, respectively, for the entire campaign in November 2012. The average rBC mass  
6 concentration is about 4 times larger for pollution episode than for clean days; and the number  
7 fraction of coated rBC particles also increases from ~~57.758%~~ for clean days to ~~64.665%~~ for  
8 pollution episode. The mass size distribution of rBC particles shows lognormal distribution  
9 with a peak diameter of  $\sim 187 \text{ nm}$  regardless of the pollution level. Back trajectory analysis  
10 and potential source contribution function (PSCF) model study show that North India is an  
11 important region influencing the rBC level in the northeastern Qinghai-Tibetan Plateau during  
12 the pollution episode. The fire counts map also suggests that the pollution episode is likely  
13 caused by biomass burning in North India.

14 The average light absorption (at  $\lambda = 532 \text{ nm}$ ) is  $1.3 \text{ Mm}^{-1}$  for the clean days and increases to  
15  $3.7 \text{ Mm}^{-1}$  for pollution episode. The rBC mass absorption cross section ( $\text{MAC}_{\text{rBC}}$ ) at  $\lambda = 532$   
16  $\text{nm}$  was larger in clean days ( $14.9 \text{ m}^2 \text{ g}^{-1}$ ) than during pollution episode ( $9.3 \text{ m}^2 \text{ g}^{-1}$ ), likely due  
17 to the effects of brown carbon and the uncertainty of the  $\text{MAC}_{\text{rBC}}$  calculation. The  $\text{MAC}_{\text{rBC}}$   
18 was positively correlated with number fraction of coated rBC during pollution episode with  
19 an increasing rate of  $0.18 (\text{m}^2 \text{ g}^{-1}) \%^{-1}$ . The number fraction of coated rBC particles shows  
20 positive correlation with light absorption, suggesting that the increase of aged rBC particles  
21 increases the light absorption. Compared to rBC mass concentration, rBC mixing state is more  
22 important in determining absorption during pollution episode, estimated from the same  
23 percentagewise increment of either rBC mass concentration or the number fraction of coated  
24 rBC. The estimated BC direct radiative forcing is about 2 times higher for pollution episode  
25 ( $0.93 \pm 0.57 \text{ W m}^{-2}$ ) than for clean days ( $0.48 \pm 0.29 \text{ W m}^{-2}$ ).

26 This case study provides an insight into the sources, mixing state and optical properties of  
27 rBC particles in the northeast Qinghai-Tibetan Plateau.~~South Asia pollution impacting~~  
28 ~~northeast Qinghai-Tibetan Plateau through long range transport.~~ The enhancement of rBC  
29 absorption not only disturbs the energy budget of the atmosphere in this region, but also  
30 modifies the snow albedo by deposition. This in turn can accelerate the melting of the glaciers  
31 and snow-pack over Qinghai-Tibetan and, thus, affect the sustaining seasonal water  
32 availability leading to security of agriculture in downstream regions. More studies need to be

1 addressed on the basis of long-period investigations in the Qinghai-Tibetan Plateau region to  
2 improve our scientific understanding of the regional climate on the inter-annual as well as  
3 intra-seasonal scale.

#### 4 **Acknowledgements**

5 This work was supported by the projects from the National Natural Science Foundation of  
6 China (41230641) and the Ministry of Science & Technology (2012BAH31B03, 201209007).

## 1 **References**

- 2 An, Z., Colman, S.M., Zhou, W., Li, X., Brown, E.T., Jull, A.J.T., Cai, Y., Huang, Y., Lu, X.,  
3 Chang, H., Song, Y., Sun, Y., Xu, H., Liu, W., Jin, Z., Liu, X., Cheng, P., Liu, Y., Ai, L.,  
4 Li, X., Liu, X., Yan, L., Shi, Z., Wang, X., Wu, F., Qiang, X., Dong, J., Lu, F., Xu, X.:  
5 Interplay between the Westerlies and Asian monsoon recorded in Lake Qinghai sediments  
6 since 32 ka, *Sci. Rep.*, 2, 619, doi: 10.1038/srep00619, 2012.
- 7 [Andreae, M.O., Gelencser, A.: Black carbon or brown carbon? The nature of light-absorbing](#)  
8 [carbonaceous aerosols, \*Atmos. Chem. Phys.\*, 6, 3131–3148, 2006.](#)
- 9 Anenberg, S.C., Schwartz, J., Shindell, D., Amann, M., Faluvegi, G., Klimont, Z., Janssens-  
10 Maenhout, G., Pozzoli, L., Van Dingenen, R., Vignati, E., Emberson, L., Muller, N.Z.,  
11 West, J.J., Williams, M., Demkine, V., Hicks, W.K., Kuylensstierna, J., Raes, F.,  
12 Ramanathan, V.: Global air quality and health co-benefits of mitigating near-term climate  
13 change through methane and black carbon emission controls, *Environ. Health Persp.*, 120,  
14 831–839, 2012.
- 15 Bonasoni, P., Laj, P., Marinoni, A., Sprenger, M., Angelini, F., Arduini, J., Bonafe, U.,  
16 Calzolari, F., Colombo, T., Decesari, S., Di Biagio, C., di Sarra, A.G., Evangelisti, F.,  
17 Duchi, R., Facchini, M.C., Fuzzi, S., Gobbi, G.P., Maione, M., Panday, A., Roccatò, F.,  
18 Sellegri, K., Venzac, H., Verza, G.P., Villani, P., Vuillermoz, E., Cristofanelli, P.:  
19 Atmospheric Brown Clouds in the Himalayas: first two years of continuous observations at  
20 the Nepal Climate Observatory-Pyramid (5079 m), *Atmos. Chem. Phys.*, 10, 7515–7531,  
21 2010.
- 22 Bond, T.C. and Bergstrom, R.W.: Light absorption by carbonaceous particles: An  
23 investigative review, *Aerosol Sci, Tech.*, 40, 27–67, 2006.
- 24 Bond, T.C., Habib, G., Bergstrom, R.W.: Limitations in the enhancement of visible light  
25 absorption due to mixing state, *J. Geophys. Res.*, 111, D20211, doi:  
26 10.1029/2006JD007315, 2006.
- 27 Bond, T.C., Doherty, S.J., Fahey, D.W., Forster, P.M., Berntsen, T., DeAngelo, B.J., Flanner,  
28 M.G., Ghan, S., Kärcher, B., Koch, D., Kinne, S., Kondo, Y., Quinn, P.K., Sarofim, M.C.,  
29 Schultz, M.G., Schulz, M., Venkataraman, C., Zhang, H., Zhang, S., Bellouin, N.,  
30 Guttikunda, S.K., Hopke, P.K., Jacobson, M.Z., Kaiser, J.W., Klimont, Z., Lohmann, U.,  
31 Schwarz, J.P., Shindell, D., Storelvmo, T., Warren, S.G., Zender, C.S.: Bounding the role



- 1 of black carbon in the climate system: A scientific assessment, *J. Geophys. Res.*, 118,  
2 5380–5552, 2013.
- 3 ~~[Browne, E.C., Franklin, J.P., Canagaratna, M.R., Massoli, P., Kirchstetter, T.W., Worsnop,](#)~~  
4 ~~[D.R., Wilson, K.R., Kroll, J.H.: Changes to the chemical composition of soot from](#)~~  
5 ~~[heterogeneous oxidation reactions, \*J. Phys. Chem. A\*, 119, 1154–1163, 2015.](#)~~
- 6 Cao, J.J., Tie, X.X., Xu, B.Q., Zhao, Z.Z., Zhu, C.S., Li, G.H., Liu, S.X.: Measuring and  
7 modeling black carbon (BC) contamination in the SE Tibetan Plateau, *J. Atmos. Chem.*, 67,  
8 45–60, 2010.
- 9 ~~[Cape, J.N., Coyle, M., Dumitrean, P.: The atmospheric lifetime of black carbon, \*Atmos.\*](#)~~  
10 ~~[Environ.](#), 59, 256–263, 2012.~~
- 11 Chung, C.E., Lee, K., Mueller, D.: Effect of internal mixture on black carbon radiative  
12 forcing, *Tellus B*, 64, 1–13, 2012.
- 13 ~~[Chung, S.H. and Seinfeld, J.H.: Climate response of direct radiative forcing of anthropogenic](#)~~  
14 ~~[black carbon, \*J. Geophys. Res.\*, 110, D11102, doi:10.1029/2004JD005441, 2005.](#)~~
- 15 Chylek, P. and Wong, J.: Effect of absorbing aerosols on global radiation budget, *Geophys.*  
16 *Res. Lett.*, 22, 929–931, 1995.
- 17 Collaud Coen, M., Weingartner, E., Apituley, A., Ceburnis, D., Fierz-Schmidhauser, R.,  
18 Flentje, H., Henzing, J., Jennings, S.G., Moerman, M., Petzold, A.: Minimizing light  
19 absorption measurement artifacts of the Aethalometer: evaluation of five correction  
20 algorithms, *Atmos. Meas. Tech.*, 3, 457–474, 2010.
- 21 Cong, Z., Kang, S., Gao, S., Zhang, Y., Li, Q., Kawamura, K.: Historical trends of  
22 atmospheric black carbon on Tibetan Plateau as reconstructed from a 150-Year lake  
23 sediment record, *Environ. Sci. Technol.*, 47, 2579–2586, 2013.
- 24 Forbes, M.S., Raison, R.J., Skjemstad, J.O.: Formation, transformation and transport of black  
25 carbon (charcoal) in terrestrial and aquatic ecosystems, *Sci. Total Environ.*, 370, 190–206,  
26 2006.
- 27 ~~[Fuller, K.A., Malm, W.C., Kreidenweis, S.M.: Effects of mixing on extinction by](#)~~  
28 ~~[carbonaceous particles, \*J. Geophys. Res.\*, 104, 15941–15954, 1999.](#)~~
- 29 Gao, R., Schwarz, J., Kelly, K., Fahey, D., Watts, L., Thompson, T., Spackman, J., Slowik, J.,  
30 Cross, E., Han, J.H.: A novel method for estimating light-scattering properties of soot

- 1 aerosols using a modified single-particle soot photometer, *Aerosol Sci, Tech.*, 41, 125–135,  
2 2007.
- 3 Hansen, J., Sato, M., Ruedy, R., Nazarenko, L., Lacis, A., Schmidt, G.A., Russell, G.,  
4 Aleinov, I., Bauer, M., Bauer, S., Bell, N., Cairns, B., Canuto, V., Chandler, M., Cheng, Y.,  
5 Del Genio, A., Faluvegi, G., Fleming, E., Friend, A., Hall, T., Jackman, C., Kelley, M.,  
6 Kiang, N., Koch, D., Lean, J., Lerner, J., Lo, K., Menon, S., Miller, R., Minnis, P.,  
7 Novakov, T., Oinas, V., Perlwitz, J., Rind, D., Romanou, A., Shindell, D., Stone, P., Sun,  
8 S., Tausnev, N., Thresher, D., Wielicki, B., Wong, T., Yao, M., Zhang, S.: Efficacy of  
9 climate forcings, *J. Geophys. Res.*, 110, D18104, doi: 10.1029/2005JD005776, 2005.
- 10 Heo, J., McGinnis, J.E., de Foy, B., Schauer, J.J.: Identification of potential source areas for  
11 elevated PM<sub>2.5</sub>, nitrate and sulfate concentrations, *Atmos. Environ.*, 71, 187–197, 2013.
- 12 Hindman, E.E. and Upadhyay, B.P.: Air pollution transport in the Himalayas of Nepal and  
13 Tibet during the 1995-1996 dry season, *Atmos. Environ.*, 36, 727–739, 2002.
- 14 Immerzeel, W.W., van Beek, L.P.H., Bierkens, M.F.P.: Climate change will affect the Asian  
15 water towers, *Science*, 328, 1382–1385, 2010.
- 16 Jacobson, M.Z.: Strong radiative heating due to the mixing state of black carbon in  
17 atmospheric aerosols, *Nature*, 409, 695–697, 2001.
- 18 Kühn, T., Partanen, A.I., Laakso, A., Lu, Z., Bergman, T., Mikkonen, S., Kokkola, H.,  
19 Korhonen, H., Räisänen, P., Streets, D.G., Romakkaniemi, S., Laaksonen, A.: Climate  
20 impacts of changing aerosol emissions since 1996, *Geophys. Res. Lett.*, 41, 4711–4718,  
21 2014.
- 22 Kim, M.Y., Lee, S.-B., Bae, G.-N., Park, S.S., Han, K.M., Park, R.S., Song, C.H., Park, S.H.:  
23 Distribution and direct radiative forcing of black carbon aerosols over Korean Peninsula,  
24 *Atmos. Environ.*, 58, 45–55, 2012.
- 25 [Koch, D. and Del Genio, A. D.: Black carbon semi-direct effects on cloud cover: review and](#)  
26 [synthesis, \*Atmos. Chem. Phys.\*, 10, 7685-7696, 2010.](#)
- 27 Kondo, Y., Matsui, H., Moteki, N., Sahu, L., Takegawa, N., Kajino, M., Zhao, Y., Cubison,  
28 M. J., Jimenez, J. L., Vay, S., Diskin, G. S., Anderson, B., Wisthaler, A., Mikoviny, T.,  
29 Fuelberg, H. E., Blake, D. R., Huey, G., Weinheimer, A. J., Knapp, D. J., Brune, W. H.:  
30 Emissions of black carbon, organic, and inorganic aerosols from biomass burning in North

- 1 America and Asia in 2008, *J. Geophys. Res.*, 116(D8), D08204,  
2 doi:10.1029/2010JD015152, 2011.
- 3 Kopacz, M., Mauzerall, D.L., Wang, J., Leibensperger, E.M., Henze, D.K., Singh, K.: Origin  
4 and radiative forcing of black carbon transported to the Himalayas and Tibetan Plateau,  
5 *Atmos. Chem. Phys.*, 11, 2837–2852, 2011.
- 6 Kurokawa, J., Ohara, T., Morikawa, T., Hanayama, S., Janssens-Maenhout, G., Fukui, T.,  
7 Kawashima, K., Akimoto, H.: Emissions of air pollutants and greenhouse gases over Asian  
8 regions during 2000–2008: Regional emission inventory in ASia (REAS) version 2, *Atmos.*  
9 *Chem. Phys.*, 13, 11019–11058, 2013.
- 10 ~~Lack, D. and Cappa, C.: Impact of brown and clear carbon on light absorption enhancement,~~  
11 ~~single scatter albedo and absorption wavelength dependence of black carbon, *Atmos.*~~  
12 ~~*Chem. Phys.*, 10, 4207–4220, 2010.~~
- 13 Liu, D., Allan, J., Whitehead, J., Young, D., Flynn, M., Coe, H., McFiggans, G., Fleming,  
14 Z.L., Bandy, B.: Ambient black carbon particle hygroscopic properties controlled by  
15 mixing state and composition, *Atmos. Chem. Phys.*, 13, 2015–2029, 2013.
- 16 Lohmann, U. and Feichter, J.: Global indirect aerosol effects: a review, *Atmos. Chem. Phys.*,  
17 5, 715–737, 2005.
- 18 Lu, Z., Streets, D.G., Zhang, Q., Wang, S.: A novel back-trajectory analysis of the origin of  
19 black carbon transported to the Himalayas and Tibetan Plateau during 1996–2010, *Geophys.*  
20 *Res. Lett.*, 39, L01809, doi: 10.1029/2011GL049903, 2012.
- 21 McMeeking, G., Morgan, W., Flynn, M., Highwood, E., Turnbull, K., Haywood, J., Coe, H.:  
22 Black carbon aerosol mixing state, organic aerosols and aerosol optical properties over the  
23 United Kingdom, *Atmos. Chem. Phys.*, 11, 9037–9052, 2011.
- 24 Ming, J., Wang, P., Zhao, S., Chen, P.: Disturbance of light-absorbing aerosols on the albedo  
25 in a winter snowpack of Central Tibet, *J. Environ. Sci.*, 25, 1601–1607, 2013.
- 26 Moteki, N. and Kondo, Y.: Effects of mixing state on black carbon measurements by laser-  
27 induced incandescence, *Aerosol Sci, Tech.*, 41, 398–417, 2007.
- 28 Perring, A., Schwarz, J., Spackman, J., Bahreini, R., de Gouw, J., Gao, R., Holloway, J., Lack,  
29 D., Langridge, J., Peischl, J.: Characteristics of black carbon aerosol from a surface oil burn  
30 during the Deepwater Horizon oil spill, *Geophys. Res. Lett.*, 38, L17809, doi:  
31 10.1029/2011GL048356, 2011.

- 1 [Ping, X., Jiang, Z., Li, C.: Status and future perspectives of energy consumption and its](#)  
2 [ecological impacts in the Qinghai-Tibet region, \*Renew. Sustain Energy Rev.\*, 15, 514–523,](#)  
3 [2011.](#)
- 4 ~~[Polissar, A.V., Hopke, P.K., Harris, J.M.: Source regions for atmospheric aerosol measured at](#)~~  
5 ~~[Barrow, Alaska, \*Environ. Sci. Technol.\*, 35, 4214–4226, 2001.](#)~~
- 6 Polissar, A.V., Hopke, P.K., Paatero, P., Kaufmann, Y.J., Hall, D.K., Bodhaine, B.A., Dutton,  
7 E.G., Harris, J.M.: The aerosol at Barrow, Alaska: long-term trends and source locations,  
8 *Atmos. Environ.*, 33, 2441–2458, 1999.
- 9 [Polissar, A.V., Hopke, P.K., Harris, J.M.: Source regions for atmospheric aerosol measured at](#)  
10 [Barrow, Alaska, \*Environ. Sci. Technol.\*, 35, 4214–4226, 2001.](#)
- 11 Ramanathan, V. and Carmichael, G.: Global and regional climate changes due to black carbon,  
12 *Nat. Geosci.*, 1, 221–227, 2008.
- 13 Sahu, S.K., Beig, G., Sharma, C.: Decadal growth of black carbon emissions in India,  
14 *Geophys. Res. Lett.*, 35, L02807, doi: 10.1029/2007GL032333, 2008.
- 15 [Sahu, L.K., Kondo, Y., Moteki, N., Takegawa, N., Zhao, Y., Cubison, M. J., Jimenez, J. L.,](#)  
16 [Vay, S., Diskin, G. S., Wisthaler, A., Mikoviny, T., Huey, L. G., Weinheimer, A. J. and](#)  
17 [Knapp, D. J.: Emission characteristics of black carbon in anthropogenic and biomass](#)  
18 [burning plumes over California during ARCTAS-CARB 2008, \*J. Geophys. Res.\*, 117\(D16\),](#)  
19 [D16302, doi:10.1029/2011JD017401, 2012.](#)
- 20 Schwarz, J.P., Gao, R.S., Fahey, D.W., Thomson, D.S., Watts, L.A., Wilson, J.C., Reeves,  
21 J.M., Darbeheshti, M., Baumgardner, D.G., Kok, G.L., Chung, S.H., Schulz, M., Hendricks,  
22 J., Lauer, A., Kärcher, B., Slowik, J.G., Rosenlof, K.H., Thompson, T.L., Langford, A.O.,  
23 Loewenstein, M., Aikin, K.C.: Single-particle measurements of midlatitude black carbon  
24 and light-scattering aerosols from the boundary layer to the lower stratosphere, *J. Geophys.*  
25 *Res.*, 111, D16207, doi: 10.1029/2006JD007076, 2006.
- 26 Schwarz, J.P., Gao, R.S., Spackman, J.R., Watts, L.A., Thomson, D.S., Fahey, D.W., Ryerson,  
27 T.B., Peischl, J., Holloway, J.S., Trainer, M., Frost, G.J., Baynard, T., Lack, D.A., de Gouw,  
28 J.A., Warneke, C., Del Negro, L.A.: Measurement of the mixing state, mass, and optical  
29 size of individual black carbon particles in urban and biomass burning emissions, *Geophys.*  
30 *Res. Lett.*, 35, L13810, doi: 10.1029/2008GL033968, 2008a.

- 1 ~~Schwarz, J.P., Spackman, J.R., Fahey, D.W., Gao, R.S., Lohmann, U., Stier, P., Watts, L.A.,~~  
2 ~~Thomson, D.S., Lack, D.A., Pfister, L., Mahoney, M.J., Baumgardner, D., Wilson, J.C.,~~  
3 ~~Reeves, J.M.: Coatings and their enhancement of black carbon light absorption in the~~  
4 ~~tropical atmosphere, *J. Geophys. Res.*, 113, D03203, doi: 10.1029/2007JD009042, 2008b.~~
- 5 Schwarz, J.P., Spackman, J.R., Gao, R.S., Watts, L.A., Stier, P., Schulz, M., Davis, S.M.,  
6 Wofsy, S.C., Fahey, D.W.: Global-scale black carbon profiles observed in the remote  
7 atmosphere and compared to models, *Geophys. Res. Lett.*, 37, L18812, doi:  
8 10.1029/2010GL044372, 2010.
- 9 Seinfeld, J.H. and Pandis, S.N.: Atmospheric chemistry and physics: From air pollution to  
10 climate change, Wiley, New York, 1998.
- 11 Shiraiwa, M., Kondo, Y., Iwamoto, T., Kita, K.: Amplification of light absorption of black  
12 carbon by organic coating, *Aerosol Sci, Tech.*, 44, 46–54, 2010.
- 13 Slowik, J.G., Cross, E.S., Han, J.H., Davidovits, P., Onasch, T.B., Jayne, J.T., Williams, L.R.,  
14 Canagaratna, M.R., Worsnop, D.R., Chakrabarty, R.K.: An inter-comparison of instruments  
15 measuring black carbon content of soot particles, *Aerosol Sci, Tech.*, 41, 295–314, 2007.
- 16 Stephens, M., Turner, N., Sandberg, J.: Particle identification by laser-induced incandescence  
17 in a solid-state laser cavity, *Appl. Optics*, 42, 3726–3736, 2003.
- 18 Su, F., Duan, X., Chen, D., Hao, Z., Cuo, L.: Evaluation of the Global Climate Models in the  
19 CMIP5 over the Tibetan Plateau, *J. Climate*, 26, 3187–3208, 2013.
- 20 ~~Taylor, J. W., Allan, J. D., Allen, G., Coe, H., Williams, P. I., Flynn, M. J., Le Breton, M.,~~  
21 ~~Muller, J. B. A., Percival, C. J., Oram, D., Forster, G., Lee, J. D., Rickard, A. R., Parrington,~~  
22 ~~M., and Palmer, P. I.: Size-dependent wet removal of black carbon in Canadian biomass~~  
23 ~~burning plumes, *Atmos. Chem. Phys.*, 14, 13755-13771, 2014.~~
- 24 ~~Taylor, J. W., Allan, J. D., Liu, D., Flynn, M., Weber, R., Zhang, X., Lefer, B. L., Grossberg,~~  
25 ~~N., Flynn, J., Coe, H.: Assessment of the sensitivity of core/shell parameters derived using~~  
26 ~~the single-particle soot photometer to density and refractive index, *Atmos. Meas. Tech.*,~~  
27 ~~8(4), 1701–1718, 2015.~~
- 28 Tollefsen, P., Rypdal, K., Torvanger, A., Rive, N.: Air pollution policies in Europe:  
29 Efficiency gains from integrating climate effects with damage costs to health and crops,  
30 *Environ. Sci. Policy*, 12, 870–881, 2009.

- 1 [Wan, X., Kang, S., Wang, Y., Xin, J., Liu, B., Guo, Y., Wen, T., Zhang, G., and Cong, Z.:  
2 Size distribution of carbonaceous aerosols at a high-altitude site on the central Tibetan  
3 Plateau \(Nam Co Station, 4730 m a.s.l.\), Atmos. Res., 153, 155-164, 2015.](#)
- 4 Wang, Q.Y., Schwarz, J.P., Cao, J.J., Gao, R.S., Fahey, D.W., Hu, T.F., Huang, R.-J., Han,  
5 Y.M., Shen, Z.X.: Black carbon aerosol characterization in a remote area of Qinghai–  
6 Tibetan Plateau, western China, *Sci. Total Environ.*, 479, 151–158, 2014a.
- 7 Wang, Q.Y., Huang, R.-J., Cao, J.J., Han, Y.M., Wang, G.H., Li, G.H., Wang, Y.C., Dai,  
8 W.T., Zhang, R.J., Zhou, Y.Q.: Mixing state of black carbon aerosol in a heavily polluted  
9 urban area of China: Implications for light absorption enhancement, *Aerosol Sci, Tech.*, 48,  
10 689–697, 2014b.
- 11 [Wang, Q., Liu, S., Zhou, Y., Cao, J., Han, Y., Ni, H., Zhang, N., Huang, R.: Characteristics of  
12 black carbon aerosol during the Chinese Lunar Year and weekdays in Xi'an, China,  
13 Atmosphere, 6, 195–208, 2015.](#)
- 14 Wang, Y.Q., Zhang, X.Y., Arimoto, R.: The contribution from distant dust sources to the  
15 atmospheric particulate matter loadings at XiAn, China during spring, *Sci. Total Environ.*,  
16 368, 875–883, 2006.
- 17 Watson, J.G., Chow, J.C., Chen, L.W.A.: Summary of organic and elemental carbon/black  
18 carbon analysis methods and intercomparisons, *Aerosol Air Qual. Res.*, 5, 65–102, 2005.
- 19 Wild, M., Ohmura, A., Makowski, K.: Impact of global dimming and brightening on global  
20 warming, *Geophys. Res. Lett.*, 34, L04702, doi: 10.1029/2006GL028031, 2007.
- 21 Xia, X., Zong, X., Cong, Z., Chen, H., Kang, S., Wang, P.: Baseline continental aerosol over  
22 the central Tibetan plateau and a case study of aerosol transport from South Asia, *Atmos.  
23 Environ.*, 45, 7370–7378, 2011.
- 24 Xu, B., Cao, J., Joswiak, D.R., Liu, X., Zhao, H., He, J.: Post-depositional enrichment of  
25 black soot in snow-pack and accelerated melting of Tibetan glaciers, *Environ. Res. Lett.*, 7,  
26 014022, doi:10.1088/1748-9326/7/1/014022, 2012.
- 27 Xu, B., Cao, J., Hansen, J., Yao, T., Joswia, D.R., Wang, N., Wu, G., Wang, M., Zhao, H.,  
28 Yang, W.: Black soot and the survival of Tibetan glaciers, *P. Natl. Acad. Sci. USA*, 106,  
29 22114–22118, 2009.

- 1 Yang, K., Wu, H., Qin, J., Lin, C., Tang, W., Chen, Y.: Recent climate changes over the  
2 Tibetan Plateau and their impacts on energy and water cycle: A review, *Global Planet.*  
3 *Change*, 112, 79–91, 2014.
- 4 Yang, M., Howell, S.G., Zhuang, J., Huebert, B.J.: Attribution of aerosol light absorption to  
5 black carbon, brown carbon, and dust in China-interpretations of atmospheric  
6 measurements during EAST-AIRE, *Atmos. Chem. Phys.*, 9, 2035–2050, 2009.
- 7 Zhang, Q., Streets, D.G., Carmichael, G.R., He, K.B., Huo, H., Kannari, A., Klimont, Z., Park,  
8 I.S., Reddy, S., Fu, J.S.: Asian emissions in 2006 for the NASA INTEX-B mission, *Atmos.*  
9 *Chem. Phys.*, 9, 5131–5153, 2009.
- 10 Zhang, R., Jing, J., Tao, J., Hsu, S.C., Wang, G., Cao, J., Lee, C.S.L., Zhu, L., Chen, Z., Zhao,  
11 Y., Shen, Z.: Chemical characterization and source apportionment of PM<sub>2.5</sub> in Beijing:  
12 seasonal perspective, *Atmos. Chem. Phys.*, 13, 7053–7074, 2013.
- 13 Zhao, S., Ming, J., Sun, J., Xiao, C.: Observation of carbonaceous aerosols during 2006–2009  
14 in Nyainqêntanglha Mountains and the implications for glaciers, *Environ. Sci. Pollut. R.*,  
15 20, 5827–5838, 2013.
- 16 Zhuang, B.L., Li, S., Wang, T.J., Deng, J.J., Xie, M., Yin, C.Q., Zhu, J.L.: Direct radiative  
17 forcing and climate effects of anthropogenic aerosols with different mixing states over  
18 China, *Atmos. Environ.*, 79, 349–361, 2013.



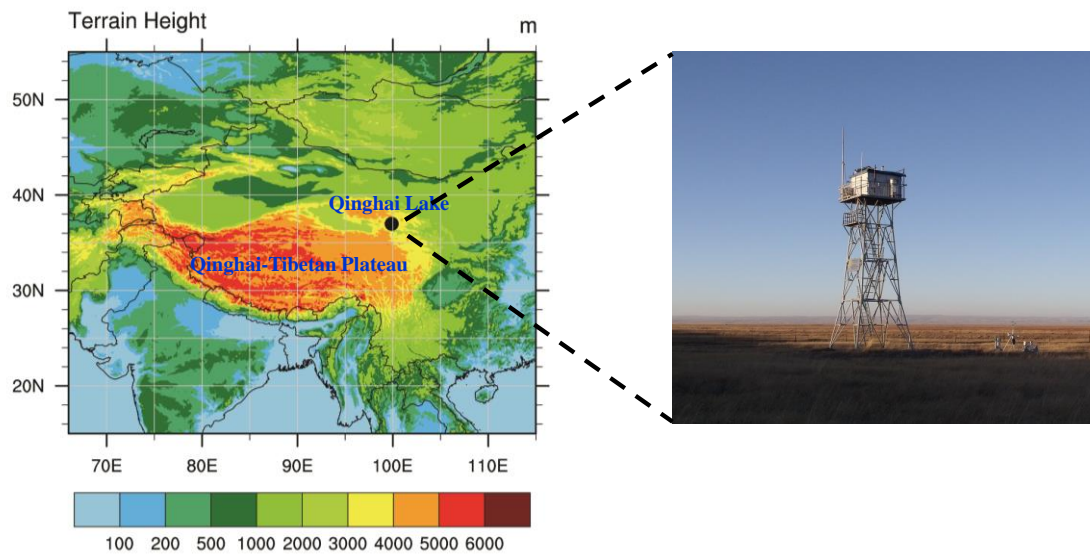
1 | Table 1 Summary of rBC concentrations, number fraction of coated rBC, light absorption coefficient, and mass absorption cross section of  
 2 | rBC (MAC<sub>rBC</sub>) during different sampling periods.

	rBC (mean ± SD, ng m <sup>-3</sup> )			Number fraction of coated rBC (%)			Absorption (Mm <sup>-1</sup> )			MAC <sub>rBC</sub> (m <sup>2</sup> g <sup>-1</sup> )		
	PE <sup>*</sup>	CD <sup>*</sup>	All	PE	CD	All	PE	CD	All	PE	CD	All
Average	390±207	86±101	160±190	65±5	58±7	59±7	3.7±2.9	1.3±1.6	2.1±2.4	9.3±3.1	14.9±8.9	13.2±8.1
25th	219	40	50	63	53	54	1.4	0.7	0.8	7.4	9.0	8.3
50th	410	68	80	66	58	60	3.4	0.9	1.2	9.0	13.6	11.2
75th	489	103	170	68	63	65	4.4	1.4	2.0	10.7	18.7	16.7

4 | <sup>\*</sup>PE and CD represent the pollution episode and clean days, respectively.

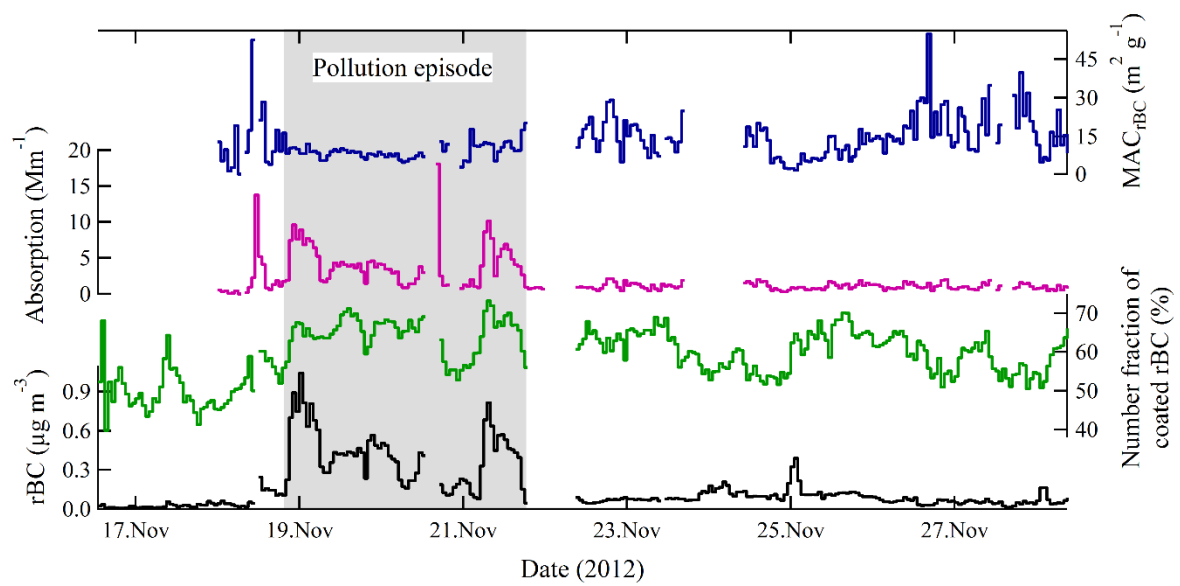
5

6



1  
2  
3  
4  
5  
6

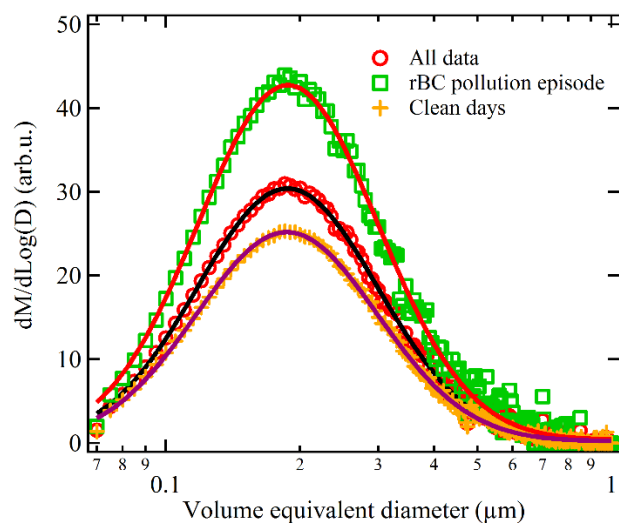
Figure 1. (left) Geographical location of Qinghai-Tibetan Plateau and surrounding areas. Color code represents topographical features (unit: m). (right) Observation tower at the “Bird Island” peninsula in Qinghai Lake, China.



1  
2  
3  
4  
5  
6  
7  
8  
9  
10  
11  
12  
13  
14  
15  
16  
17  
18

Figure 2. Time series of the rBC mass concentration, number fraction of coated rBC, light absorption at  $\lambda = 532$  nm, and mass absorption cross section of rBC ( $MAC_{rBC}$ ) during the entire campaign period. The pollution episode is highlighted with grey background.

1



2

3

4 | Figure 3. Mass size distribution of rBC in volume equivalent diameter during different  
5 | sampling periods at Qinghai Lake. The solid lines represent lognormal fit. “M” and “D” in  
6 | vertical label represent rBC mass and void free diameter (assuming  $2 \text{ g cm}^{-3}$  density),  
7 | respectively.

8

9

10

11

12

13

14

15

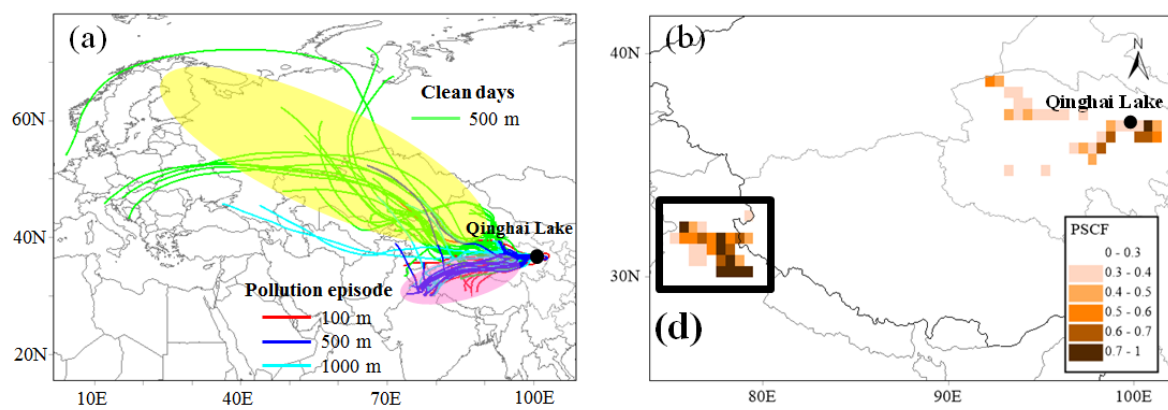
16

17

18

19

1



2

3

4 | Figure 4. (a) Five-day backward air mass trajectories reaching at Qinghai Lake at 100, 500  
5 | and 1000 m above ground every six hours and (b) Likely source areas of rBC identified using  
6 | potential source contribution function (PSCF) plots during the entire campaign.

7

8

9

10

11

12

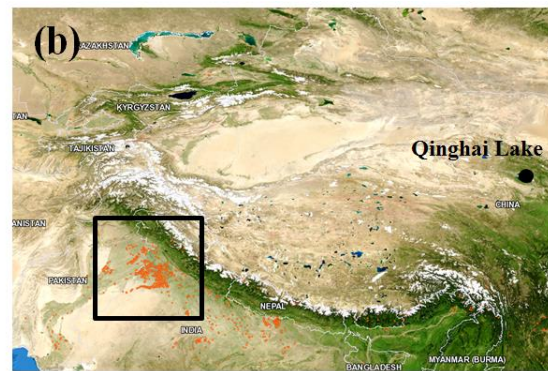
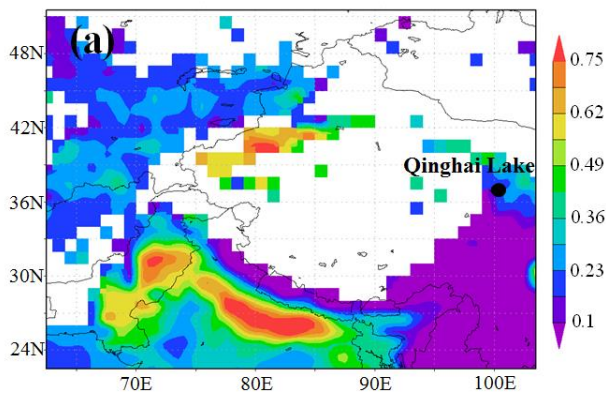
13

14

15

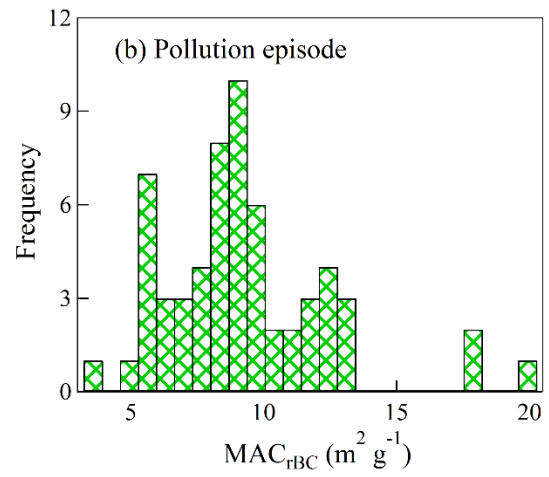
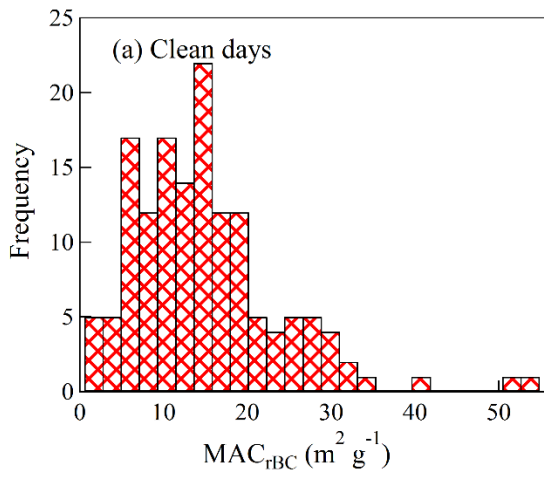
16

17



1  
2  
3  
4  
5  
6  
7  
8  
9  
10  
11  
12  
13  
14  
15

Figure 5. Regional distributions of (a) aerosol optical depth (AOD) and (b) fire counts map over Qinghai-Tibetan Plateau derived from MODIS observation during 16–27 November, 2012.



1

2

3 Figure 6. Frequency distributions of rBC mass absorption cross section (MAC<sub>rBC</sub>) during (a)  
 4 clean days and (b) pollution episode.

5

6

7

8

9

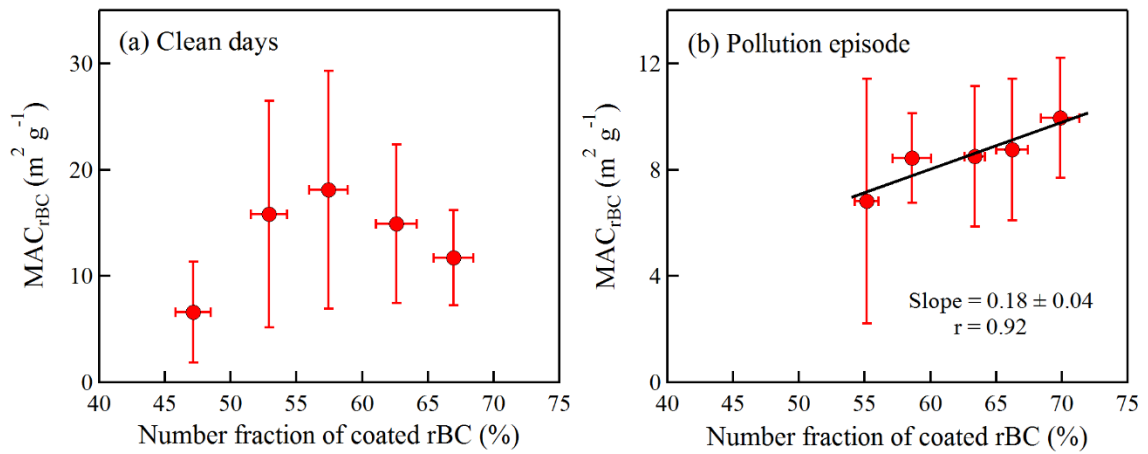
10

11

12

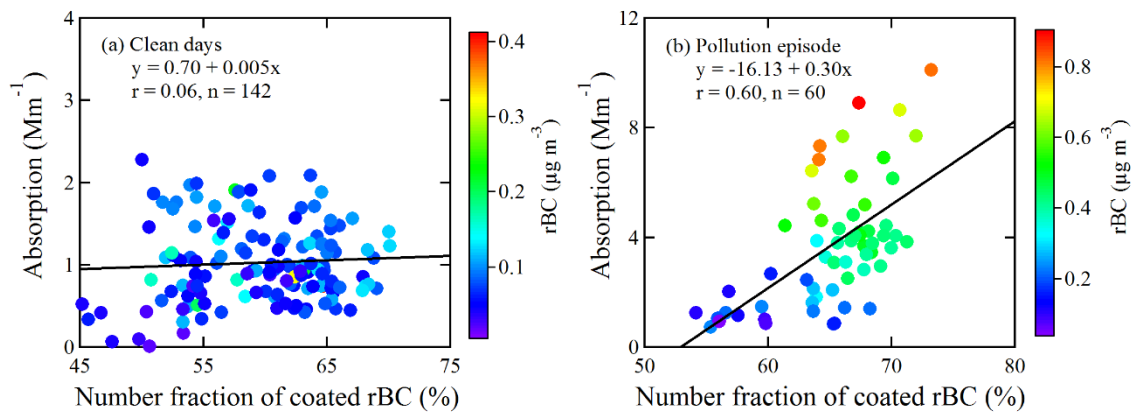
13





1  
2  
3  
4  
5  
6  
7  
8  
9  
10  
11  
12  
13  
14

Figure 7. Mass absorption cross section of rBC ( $MAC_{rBC}$ ) versus number fraction of coated rBC during (a) clean days and (b) pollution episode. The error bars correspond to the standard deviations of  $MAC_{rBC}$  and number fraction of coated rBC.



1  
 2  
 3  
 4  
 5

Figure 8. Light absorption as a function of number fraction of coated rBC during (a) clean days and (b) pollution episode. Data points are color coded for rBC mass concentration.